Research Square

Preprints are preliminary reports that have not undergone peer review.
They should not be considered conclusive, used to inform clinical practice,
or referenced by the media as validated information.

Tandem Effect Of Decursin And Enzalutamide Co-Delivered By Elastin Nanogel In Prostate Cancer Xenografts

Jonathan Yeshwanth Daniel
Sri Ramachandra Institute of Higher Education & Research
Gulzar Ahmed Rather
Sri Ramachandra Institute of Higher Education & Research
R Siva
Sri Ramachandra Institute of Higher Education & Research
K. Natarajan
Sri Ramachandra Institute of Higher Education & Research
K Sathish Srinivas
Sri Ramachandra Institute of Higher Education & Research
Ravindran Jaganathan
Universiti Kuala Lumpur, Royal College of Medicine Perak
Vinoth-Kumar Lakshmanan
vinoth.lakshmanan@sriramachandra.edu.in

Sri Ramachandra Institute of Higher Education & Research

Article

Keywords: Prostate cancer, Elastin, Castration resistance, Xenograft, Zebrafish, Global oncology

Posted Date: March 25th, 2026

DOI: https://doi.org/10.21203/rs.3.rs-9057482/v1

License: This work is licensed under a Creative Commons Attribution 4.0 International License.
Read Full License

Additional Declarations: No competing interests reported.

Tandem Effect Of Decursin And Enzalutamide Co-Delivered By Elastin Nanogel In Prostate Cancer Xenografts

Jonathan Yeshwanth Daniel[1], Gulzar Ahmed Rather[1], Siva R[2], K. Natarajan[3], K Sathish Srinivas[4], Ravindran Jaganathan[5], Vinoth-Kumar Lakshmanan[1,6]*

[1]Prostate Cancer Biomarker Laboratory, Faculty of Clinical Research, Sri Ramachandra Institute of Higher Education & Research, Porur, Chennai 600116, India.

[2]Centre for Toxicology and Developmental Research, Sri Ramachandra Institute of Higher Education & Research, Porur, Chennai 600 116, India.

[3]Department of Radiation Oncology, Faculty of Medicine, Sri Ramachandra Institute of Higher Education & Research, Porur, Chennai 600 116, India.

[4]Department of Urology, Faculty of Medicine, Sri Ramachandra Institute of Higher Education & Research, Porur, Chennai 600 116, India.

[5]Preclinical Department, Faculty of Medicine, Universiti Kuala Lumpur, Royal College of Medicine Perak, 30450 Ipoh, Perak, Malaysia

[6]Department of Mechanical, Industrial and Mechatronics Engineering, Faculty of Engineering and Architectural Science, Toronto Metropolitan University, Toronto, ON M5B 2K3, Canada

*email: vinoth.lakshmanan@sriramachandra.edu.in

Abstract

Prostate cancer frequently develops resistance to androgen receptor-targeted therapies such as enzalutamide, underscoring the need for rational combination strategies that exploit complementary mechanisms while improving delivery and tolerability. Here, we investigated the tandem therapeutic potential of decursin—a natural coumarin with documented anti-proliferative, anti-androgenic, and pathway-modulating effects in prostate cancer—co-delivered with enzalutamide via a biocompatible elastin-based nanogel. In silico predictions using ProTox and STITCH confirmed favorable toxicity profiles and minimal adverse interaction risks for the combination, supporting its preclinical advancement. In vivo toxicity assessments in zebrafish embryos and Sprague-Dawley rats revealed negligible systemic toxicity at therapeutic doses, with only mild, reversible, dose-dependent liver function perturbations at higher exposures. The core efficacy evaluation utilized DU145 human prostate cancer cells, a well-established model of aggressive, androgen-independent disease in athymic nude mouse xenografts. The elastin nanogel-co-loaded formulation elicited a considerable reduction in tumor volume and burden compared to free drugs or monotherapy controls, demonstrating clear tandem synergy and superior anti-tumor activity. These findings highlight the elastin nanogel as an effective platform for overcoming enzalutamide resistance through synergistic pathway targeting, offering a promising translational strategy for castration-resistant prostate cancer with an excellent safety margin.

Keywords: Prostate cancer, Elastin, Castration resistance, Xenograft, Zebrafish, Global oncology

Introduction

Metastatic castration-resistant prostate cancer (mCRPC) is an advanced and aggressive form of prostate cancer (PCa), characterized by its steady progression despite androgen deprivation therapy (ADT). Enzalutamide, a second-generation androgen receptor antagonist, has significantly improved treatment outcomes for mCRPC patients[1–3]. Patients eventually develop resistance to EZA through a variety of mechanisms which pose a challenge in prostate cancer therapy. Emergence of AR splice variants like AR-V7, which confer constitutive activity independent of ligand binding[4], altered steroidogenesis, bypass signaling pathways, or the overexpression of efflux transporters that reduce intracellular drug concentrations contribute to resistance[5]. Furthermore, AR gene aberrations, such as copy number gains and mutations, perturbations in sphingolipid metabolism leading to elevated ceramides, and activation of pathways like NOTCH signaling, can all contribute to enzalutamide resistance[6,7]. The urgency to overcome these mechanisms of resistance necessitates the exploration of innovative therapeutic strategies[7]. Added to these, hereditary factors influence prostate cancer [8,9] Our study proposes a unique co-delivery system utilizing an elastin nanogel carrier for enzalutamide and decursin, aiming to circumvent these challenges and enhance therapeutic efficacy in a DU145 xenograft model within BALB/c mice[10,11]. Nanomedicines, particularly stimuli-responsive prodrug-based nanocarriers, offer a promising avenue for improved drug delivery to tumor sites by enabling controlled drug release and overcoming biological barriers. Such nanocarriers, including nanogels, are designed to reduce systemic toxicity and improve targeting efficiency, although challenges remain in their clinical translation due to issues like systemic accumulation and manufacturing quality[12]. The proposed elastin nanogel, engineered for controlled and sustained release, aims to improve the pharmacokinetic profile of both drugs, thereby enhancing their synergistic therapeutic effects while potentially mitigating systemic toxicity. This approach is designed to maximize drug accumulation within the tumor microenvironment, increasing localized therapeutic concentrations and overcoming dose-limiting toxicities often associated with systemic administration. The DU145 cell line, an androgen-independent human prostate cancer cell line, is particularly suitable for modeling castration-resistant prostate cancer due to its established metastatic potential and resistance to androgen deprivation[13]. However, for xenograft studies involving human cancer cell lines like DU145, immunocompromised models such as athymic nude mice or SCID mice are typically preferred to prevent host immune rejection of the grafted tumor cells[14]. Therefore, a careful consideration of the immune status of the mouse model is crucial for the successful engraftment and subsequent analysis of human cancer xenografts[15]. Given that DU145 cells are of human origin, employing immunocompromised BALB/c nude mice would be a more appropriate choice to facilitate successful tumor engraftment and growth for evaluating therapeutic interventions[16]. Beyond mammalian models, zebrafish embryos and adult fish are emerging as valuable in vivo models for cancer research, including toxicity studies, compound screening, and drug repositioning, due to their rapid tumor formation, transparency, and pharmacokinetic

similarities to humans[17]. The proposed co-delivery strategy, leveraging the elastin nanogel, seeks to overcome enzalutamide resistance mechanisms by enhancing the intracellular accumulation of enzalutamide while simultaneously utilizing decursin's multi-targeted anti-cancer properties to modulate alternative survival pathways[13]. Decursin is a phytocompound with known therapeutic effects, especially in anticancer studies, where it has been widely investigated in various mouse models, including BALB/c nude mice[18]. Its mechanism of action involves inhibiting androgen receptor signaling and inducing apoptosis, thereby enhancing the cytotoxic effects of enzalutamide[19]. Alternate mechanisms involve modulating NF-kB and STAT3 pathways, which are frequently dysregulated in CRPC and contribute to drug resistance and disease progression[20,21]. This multi-targeted approach is crucial as studies have shown that inhibiting key signaling pathways, such as the ceramide-S1P axis with sphingosine kinase inhibitors, can significantly enhance enzalutamide efficacy in prostate cancer cells, suggesting that combining AR inhibition with other targeted therapies can circumvent resistance. Furthermore, the continued inhibition of androgen signaling has been demonstrated to improve the efficacy of other chemotherapeutic agents like cabazitaxel, even in enzalutamide-resistant prostate cancer models, by enhancing apoptosis[22]. This highlights the potential benefit of maintaining AR suppression while introducing synergistic compounds like decursin to further overcome resistance. Decursin's ability to inhibit cellular proliferation and angiogenesis through mechanisms distinct from enzalutamide could provide a crucial complementary therapeutic advantage, particularly in overcoming the complex, multi-factorial resistance observed in CRPC[11] The nanoscale dimensions of the elastin nanogel facilitate enhanced permeability and retention in tumor tissues, ensuring targeted delivery and higher localized drug concentrations [19]. Moreover, the inherent biocompatibility and biodegradability of elastin-based nanogels ensure minimal immunogenicity and facilitate their safe clearance from the body, further underscoring their suitability for clinical translation[23].

This combination therapy, delivered via an optimized nanogel, is hypothesized to provide a superior therapeutic outcome compared to single-agent treatments, addressing the complex resistance landscape of metastatic CRPC by modulating diverse molecular targets[24]. Apart from testing efficacy in treatment, the elastin nanogel loaded combination of drugs will also be assessed for toxicity in various organs and tissues through histological examination and blood biochemistry analyses to ensure their safety and tolerability in vivo. A preliminary acute toxicity study was conducted on rats to establish a maximum tolerated dose and to identify any immediate adverse reactions to the nanogel formulation. Further, developmental toxicity was also assessed using zebrafish embryos. The results from these preclinical safety assessments, including the evaluation of potential off-target effects and immunogenicity, are crucial for advancing this nanogel-based co-delivery system towards clinical translation[25]. This rigorous preclinical investigation aims to provide a robust data set supporting the potential clinical translation of this innovative nanogel-based co-delivery system, offering a promising new therapeutic avenue for advanced prostate cancer[19,26,27]. The multifunctional capacity of these nanostructures, combining targeted delivery with a synergistic drug combination, highlights their potential for addressing complex and heterogeneous diseases like cancer[28].

MATERIALS AND METHODS

Elastin nanogel preparation and drug loading

A stock solution of each drug was prepared by dissolving 1 mg of the drug in 1 mL of solvent (methanol for enzalutamide, ethanol for decursin). From the prepared stock, 200 µL was added to 3.8 mL of Tris buffer (50 mM, pH 8.8) along with 100 mg of elastin nanogel. The mixture was stirred at 300 rpm for 2 hours to facilitate drug loading. Following incubation, the drug-loaded nanogel was collected by centrifugation at 3050g for 30 minutes. The obtained pellet was stored at 4°C for further analysis and use. The aqueous phase is prepared in ice-cold conditions with the help of a gel pack. To 100 mg of elastin powder, 20 ul each of DCM and DMSO are added (1:1 ratio). In 1 mL of Tris buffer, BS3 is dissolved. This is then added to the elastin/DMSO/DCM mixture and stirred to form a solution. [DMSO and DCM enable the dissolution of elastin, which is hydrophobic, in Tris buffer.] The solution is stirred for 5 to 10 minutes to allow crosslinking of elastin by BS3. To 4 mL of n-hexane, while stirring, a 3:1 ratio of Span80 (600 µl) and Tween80 (200 µl) is added. The mixture is sonicated in a bath sonicator for 4 minutes to create an even mixture. While stirring the organic phase vigorously (@ 250 rpm) the aqueous phase is added dropwise, ensuring thickening of the mixture before further aqueous phase is added. Eventually, a thick white/off-white emulsion is formed, which is then dispersed by a probe sonicator (Sonics Vibra-Cell™) at 50% amplitude for 2 minutes. The emulsion is continuously stirred for 60 minutes. To quench unreacted BS3, 2 mL of 50 mM Tris is added and let sit for 15 minutes. After this, the mixture is centrifuged @4000rpm for 30 minutes. The supernatant is discarded, and the pellet (a thick white/cream coloured gel) is collected and washed using n-hexane first, followed by PBS wash(twice) and two washes with Milli-Q® water. After washing, the gel is transferred to a dialysis membrane and stirred continuously in 50 mM Tris buffer for 24 hours. The gel is collected and stored at 4 degrees Celsius. A stock solution of the drug was prepared by dissolving 1 mg of enzalutamide in 1 mL of methanol or 1 mg of decursin in 1 mL of ethanol. To load the desired drug, 200 µL of the respective stock solution was added to 3.8 mL of 50 mM Tris buffer (pH 8.8) containing 100 mg of elastin nanogel. The mixture was stirred at 300 rpm for 2 hours to facilitate drug loading. After incubation, the suspension was centrifuged at 3050 g for 30 minutes. The resulting pellet, containing the drug-loaded elastin nanogel, was collected and stored at 4°C for further use."

Bioinformatics analysis

To better understand the association and synergy of enzalutamide and decursin, STITCH analysis was done. Based on the output of STITCH associated enzymes and receptors were considered for docking with decursin. Enzalutamide's association with AR and its docking affinity has been previously established with a very good binding score of -10.98. The docking was performed using 'mcule' online. PDB files were checked for ligand binding coordinates on PyMol for targets that were not available on search, and directly detected by mcule for targets that were available on search. The one click docking module on mcule was used for this purpose. Further the probabilities of toxicities of EZA and DEC were assessed on ProTox.

Zebrafish Acute Toxicity Assessment

Zebrafish maintenance and embryo collection

Adult wild-type zebrafish (*Danio rerio*) were maintained in a stand-alone recirculating system at 28 ± 0.5 °C under a 14 h light / 10 h dark photoperiod. Breeding was performed in spawning tanks the evening before the experiment. Embryos were collected within 0–4 h post-fertilization (hpf), rinsed with embryo medium (E3: 5 mM NaCl, 0.17 mM KCl, 0.33 mM $CaCl_2$, 0.33 mM $MgSO_4$, 0.0002 % methylene blue), and staged under a stereomicroscope. Only embryos showing normal development were selected for testing.

Exposure conditions

At 4–6 hpf, embryos were randomly assorted in 6-well plates (20 embryos per well) containing 5 mL of test solution. The loaded nanogel was freshly dispersed in E3 embryo medium by bath sonication (30 s, 40 kHz) immediately before use. Serial dilutions were prepared to obtain final concentrations in the nanogram and microgram per mL range. A vehicle control (E3 medium alone) and, a positive control (2% DMSO) were considered for the study. Exposure solutions were not renewed during the test (static conditions).

Observation and endpoints

Embryos/larvae were examined under a stereomicroscope at 24, 48, 72, and 96 hpf. Developmental and morphological abnormalities were recorded according to OECD Guideline 236 (Fish Embryo Acute Toxicity Test, 2013). The following apical endpoints were scored at each time point: Coagulation of the embryo, lack of somite formation, non-detachment of the tail from the yolk sac, lack of heartbeat and lack of spontaneous movement (at 24 hpf). At 96 hpf, the following additional malformations were recorded in hatched larvae: Edema (pericardial/yolk sac), spinal curvature (lordosis, scoliosis, kyphosis), craniofacial deformities, fin malformations, pigmentation defects. Mortality was defined as the occurrence of at least one of the four lethal endpoints listed above. Photographs were taken using a Leica Thunder microscope.

Acute toxicity:

Animals

Healthy adult Wistar rats (150–200 g) were obtained from the Central Animal Facility. Animals were housed in polypropylene cages (5 animals/cage) under standard environmental conditions (temperature 22 ± 3 °C, relative humidity 50–70 %, 12-h light/dark cycle) with free access to standard pellet diet and filtered water. Animals were acclimatized for 7 days prior to the start of the experiment. All experimental procedures were approved by the Institutional Animal Ethics and conducted in accordance with CPCSEA guidelines (India) or equivalent national regulations.

Test Item and Formulation

The test item (TI), nano formulation of elastin gel loaded with combination of enzalutamide and decursin. On the day of administration, the test item was dispersed in PBS to achieve the desired concentrations. Fresh formulations were prepared immediately before use.

Experimental Design

The acute intraperitoneal toxicity study was conducted using four graded dose levels. Animals were randomly allocated to four groups (n = 5 males per group) as shown in Table 1.

A single intraperitoneal injection was administered in the lower left or right quadrant of the abdomen using a 26-gauge needle. The injection site was swabbed with 70 % isopropyl alcohol prior to injection. Each animal received the respective dose of the test item in a constant dose volume of 2 mL/kg body weight, calculated based on the most recent body weight (Day 0).

Table 1: Animal allocation for Acute toxicity assessment of combo drug delivery

Group	Treatment	No. of Animals	Animal Nos.
G1	Low dose (2.5 mg/kg)	5 males	1–5
G2	Mid dose (5.0 mg/kg)	5 males	6–10
G3	Intermediate dose (10.0 mg/kg)	5 males	11–15
G4	High dose (20.0 mg/kg)	5 males	16–20

Observations

Clinical observations: Animals were observed for signs of toxicity at 30 min, 1 h, 2 h, and 4 h post-dosing on Day 1, and once daily thereafter for 14 days. Observations included changes in skin, fur, eyes, mucous membranes, respiratory, circulatory, autonomic and central nervous system activity, somatomotor activity, and behavior pattern. Particular attention was paid to tremors, convulsions, salivation, diarrhea, lethargy, sleep, and coma.

Mortality and morbidity: Checked twice daily during the acclimatization period and throughout the 14-day observation period. Body weight: Recorded on Day 0 (prior to dosing), Day 7, and Day 14. Dose volume calculation: Dose volume (mL) = [Body weight (g) × Desired dose (mg/kg)] / [Concentration of test item (mg/mL)]. At the end of the 14-day observation period, all surviving animals were euthanized by CO_2 overdose, and gross pathological examination was performed.

Data Analysis

Mortality data were used to estimate the approximate lethal dose. Clinical signs and body-weight changes were evaluated descriptively

In Vivo Antitumor Efficacy in DU145 Prostate Cancer Xenograft Model

Animals

Male BALB/c nude mice (6–8 weeks old, 20–24 g) were obtained from an authorized breeder. Animals were housed in individually ventilated cages under specific pathogen-free conditions in the institutional animal facility at 22 ± 2 °C, 50 ± 10 % relative humidity, and a 12-h light/dark cycle. Sterile rodent diet and acidified water were provided ad libitum. All procedures were approved by the Institutional Animal Ethics and performed in accordance with national and international guidelines for the care and use of laboratory animals.

Cell line and culture conditions

Human prostate carcinoma DU145 cells were obtained from the American Type Culture Collection (ATCC® HTB-81™) and cultured in RPMI-1640 medium supplemented with 10 % fetal bovine serum and 1 % penicillin–streptomycin at 37 °C in a humidified 5 % CO_2 atmosphere. Cells were authenticated by short-tandem repeat profiling and confirmed mycoplasma-free before use.

Tumor inoculation

Exponentially growing DU145 cells were harvested, washed, and resuspended in ice-cold phosphate-buffered saline (PBS). The cell suspension was mixed 1:1 (v/v) with ice-cold Corning® Matrigel® Basement Membrane Matrix (phenol red-free). A total of 2.5×10^6 cells in 200 µL were injected subcutaneously into the right flank of each mouse using a 27-gauge needle. Tumor growth was monitored three times weekly by measuring length (L) and width (W) with digital Vernier calipers. Tumor volume was calculated using the formula:

$$\text{Tumor volume } (mm^3) = (L \times W^2) \times 0.52$$

Randomization and treatment

When mean tumor volume reached approximately 100–150 mm^3 (designated as Day 0), mice were randomized into treatment groups (n = 6–8 per group) to ensure equivalent mean tumor volumes across groups (Table 2). Treatments were administered intravenously via the lateral tail vein twice weekly (biweekly) for 28 days. The vehicle control group received sterile PBS (5 mL/kg). Test articles (blank nanogel, free drug, or drug-loaded nanogel) were freshly dispersed in PBS and administered at a dose of 10 mg/kg body weight (dose expressed as drug equivalent for loaded formulations). Body weight and clinical signs were monitored throughout the study.

Table 2:Grouping of xenografted mice for treatment

Group	Treatment	Number of Animals
G1	Control (0.5mL/kg, PBS-Vehicle)	6
G2	Nanogels (NG)	6
G3	NG + Enzulatamide (10mg/kg)	6
G4	NG + Decursin (10mg/kg)	6
G5	NG + Combo (10mg/kg)	6

Endpoint measurements

Tumor dimensions and body weight were recorded three times per week until Day 28. On Day 28, mice were euthanized by cervical dislocation under isoflurane anesthesia. Blood was collected by cardiac puncture for serum biochemistry (ALT, AST, creatinine, urea) and complete blood count analysis. Tumors were excised, weighed, photographed, and divided: one portion fixed in 10% neutral-buffered formalin for histopathology and immunohistochemistry; the remaining portion snap-frozen in liquid nitrogen for subsequent molecular analyses. Major organs (heart, liver, spleen, lungs, kidneys) were harvested, weighed, and fixed for histopathological examination.

Statistical analysis

Tumor growth curves were compared using two-way ANOVA test. Survival was evaluated by Kaplan–Meier analysis using Graphpad Prism 10.

RESULT:

Characterization: Affirmation of composition and size of the nano formulation was ascertained by FTIR spectroscopy and DLS. Results displayed in Figure 1 show the FTIR peaks for elastin nanogel and the drug loaded variants. An overlap of the peaks across all groups represents the elastin nanogel while characteristic peaks for enzalutamide and decursin are observed individually on the charts. The combination drug loaded nanogel also presents the overlap of both enzalutamide and decursin suggesting presence in the encapsulated preparation. DLS assessed hydrodynamic radii of the same present similar sizes at around 160nm on average (Figure 2).

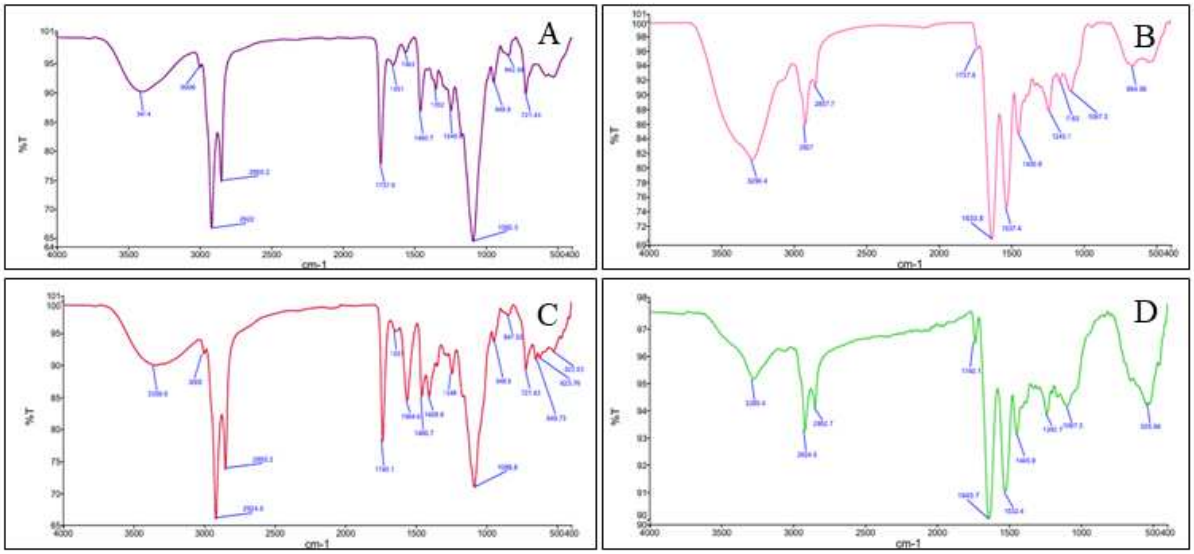


Figure 1: Fourier Transform Infrared spectrometry images of ENG(A), EZA+ENG(B), DEC+ENG (C) and COMBO+ENG(D)

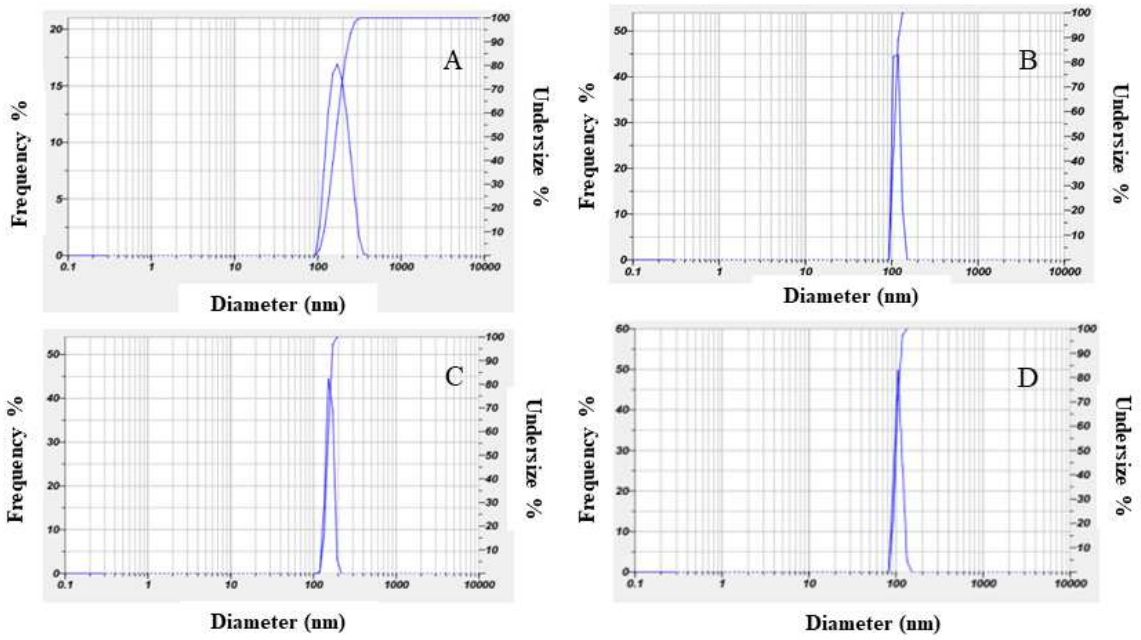


Figure 2: Hydrodynamic diameter of ENG (A) along with its drug loaded preparations viz, EZA+ENG (B), DEC+ENG (C), COMBO+ENG(D) as seen using DLS

Bioinformatics analysis: STITCH analysis produced a network of probable association between EZA and DEC. Heavier lines denote stronger association while lighter lines indicate possible association. AR appears to strongly interact with EZA and CTNNB1 and KLK3. Also and indirect influence on MMP9 and CCL2 via CTNNB1 is observed (Fig.3). Hence inhibition of AR would result in downstream effect on cellular proliferation and plasticity- which is EZA's intended purpose. DEC on the other hand shows several direct associations with CTNNB1, MMP9 and AR with moderate values while showing possible association with PARP1 and ANGPT2, suggestive of a network disrupter activity which may help overcome resistance to EZA.

Docking analysis done with DEC on *mcule* yielded results suggestive of DEC interaction pattern as predicted with STITCH. The panel of protein structures from PDB that decursin could possibly interact with were of AR (PDB ID- 1E3G, 3RLL, 3B68 and 1GS4), MMP9 (PDB ID- 1GKC). The results suggested moderate to strong binding of DEC with binding to AR ranging from -5.9(lowest with 1E3G) to -8.3 (highest) with 3RLL. With 1GKC DEC showed a binding score of -8.9.

Further toxicity assessment of DEC and EZA that were performed on ProTox (Fig.4) suggested that the relative toxicities of both drugs were low on most indexes. However, EZA does show higher respiratory toxicity along with probable hepatotoxicity and neurotoxicity. EZA is also

known to breach the BBB. DEC on the other hand showed relatively low respiratory toxicity and also breaches the BBB but has neuroprotective effect in contrast to EZA.

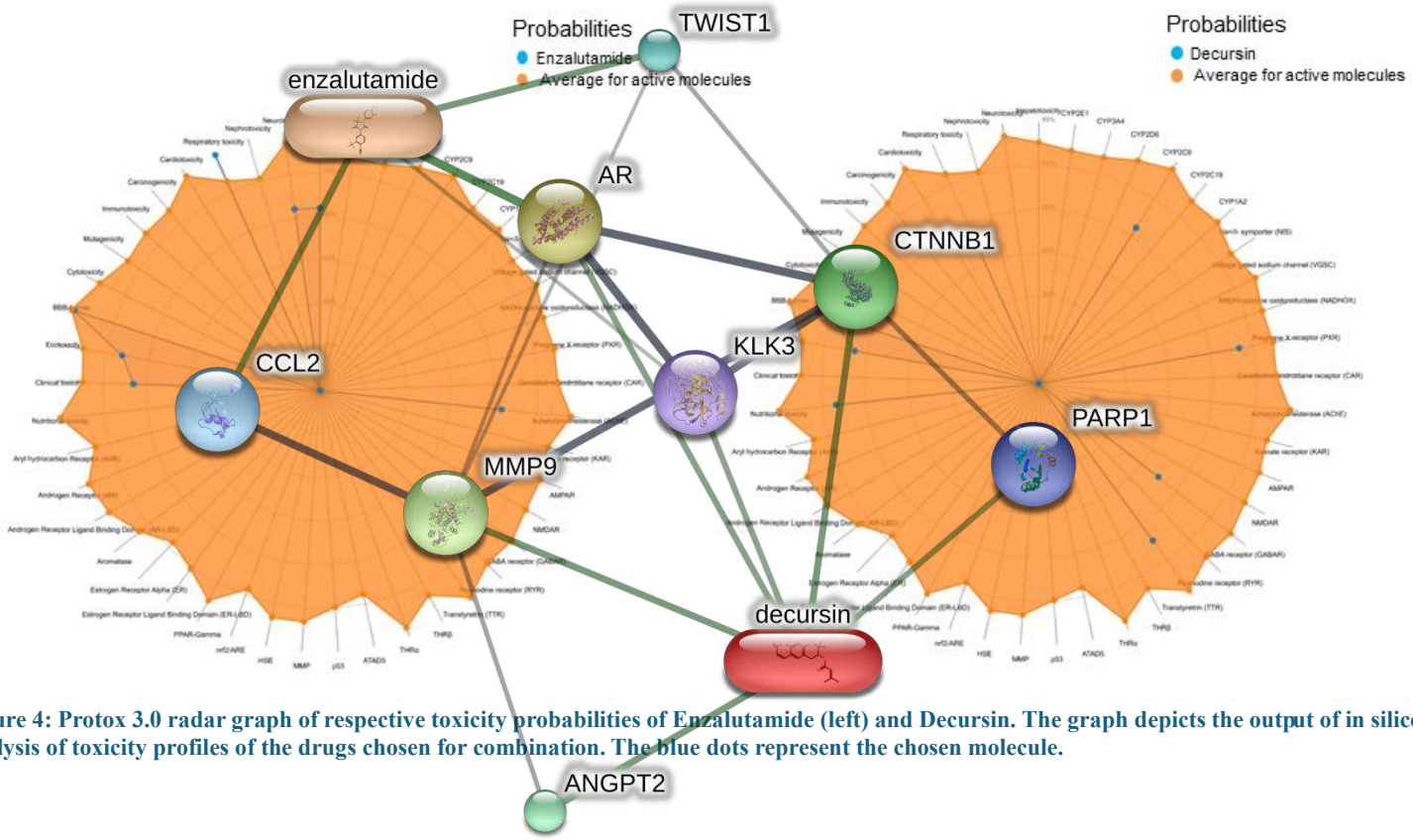


Figure 4: Protox 3.0 radar graph of respective toxicity probabilities of Enzalutamide (left) and Decursin. The graph depicts the output of in silico analysis of toxicity profiles of the drugs chosen for combination. The blue dots represent the chosen molecule.

Figure 3:STITCH output of Enzalutamide and Decursin showing probable association

Zebrafish Developmental Toxicity: Mortality and hatching were study end points for the zebrafish toxicity assessment. Results suggested that at the observed concentrations there was insignificant mortality. No developmental defects were noted during the period of observation. Photomicrographs of embryos at all times periods during the study up to 96 h are displayed in Fig.5 & 6. There was no significant toxicity observed in all concentrations when compared to control

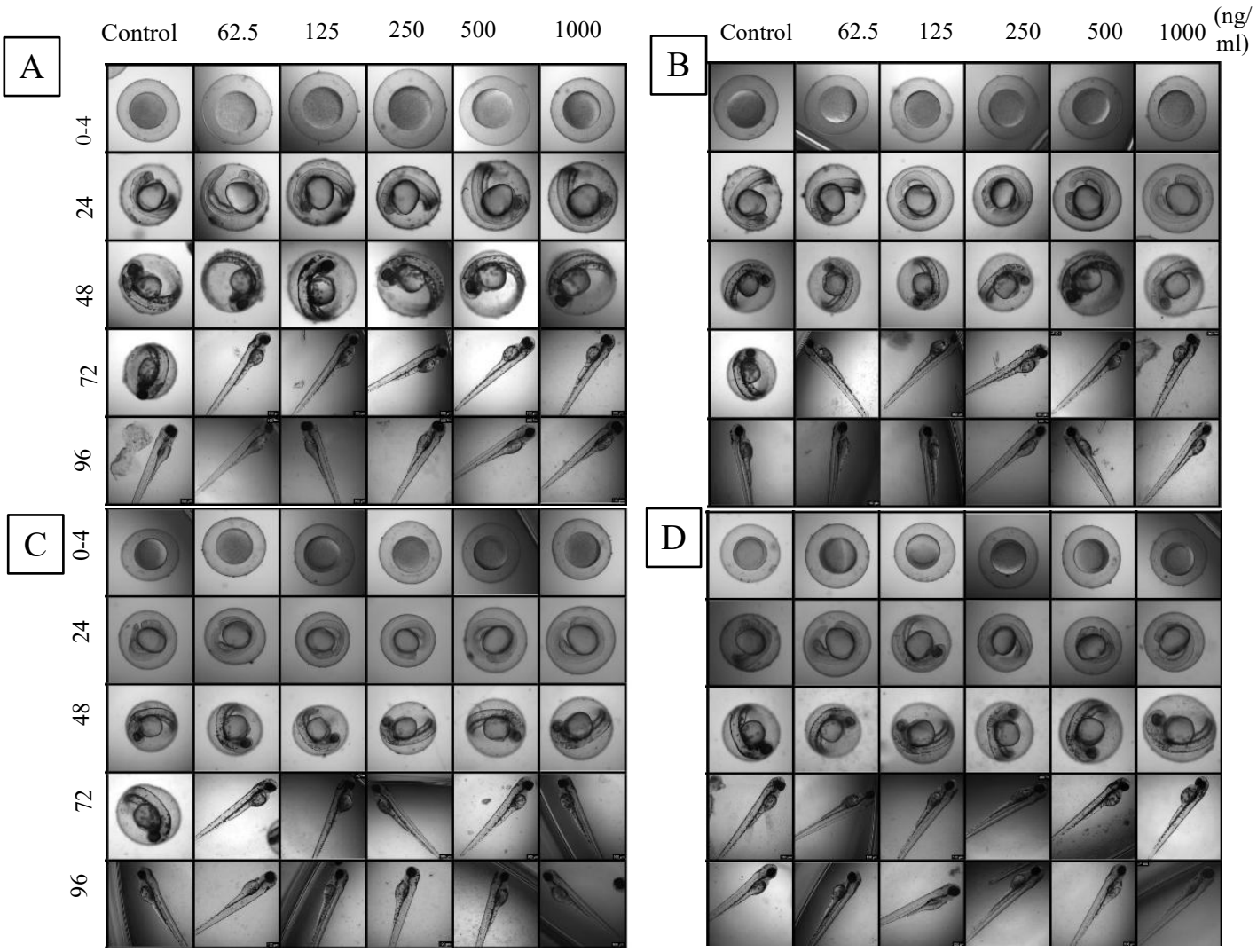


Figure 5: Photomicrographs of zebrafish embryos up to 96 hours post fertilization (hpf). A, B, C, D are treated with ENG, EZA+ENG, DEC+ENG and COMBO+ENG respectively across a panel of concentrations in nanograms per ml (ng/ml)

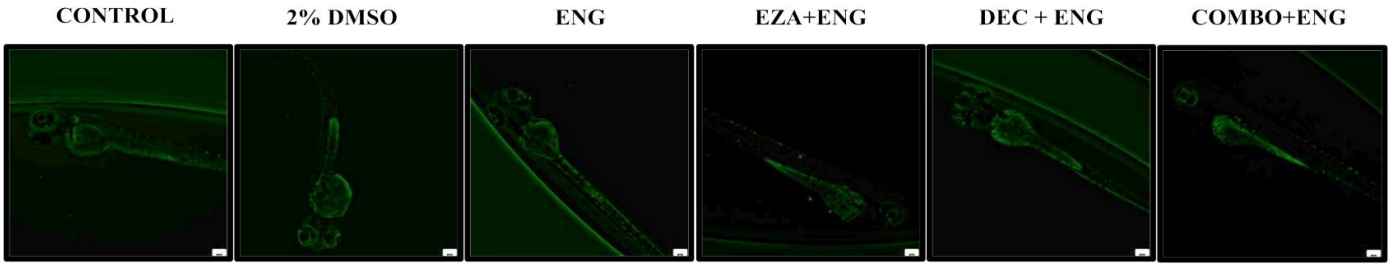


Figure 6: Acridin orange - propidium iodide (AOPI) stained preparation of zebrafish larvae at 96 hpf. Images compare negative control to positive control (2% DMSO) and treatnent groups at 20 µg/ml

Acute toxicity in rats:

Sprague Dawley rats were randomly grouped and were administered combo drug loaded nanogel intra peritoneally. Four different test doses that were considered showed no signs of toxicity- mortality and morbidity. The site of administration was observed for signs of edema and erythrema. This too showed that the drug loaded elastin nanogel caused no minimal/adverse allergic reaction. Gross pathology observation of heart, kidneys, liver, brain, lungs, thymus and abdominal organs revealed no lesions or abnormalities. It was safe to infer that there was no toxicity induced by the formulation upto 20mg/kg body weight dosage.(Tables 3 & 4)

Table 3:Observation of mortality and morbidity in rats

GROUP No: (mg/kg; b.wt)	ANIMAL No.	EXPERIMENTAL DAYS						
		1	2	3	4	5	6	7
G1: 2.5	1	X	X	X	X	X	X	X
	2	X	X	X	X	X	X	X
	3	X	X	X	X	X	X	X
	4	X	X	X	X	X	X	X
	5	X	X	X	X	X	X	X
G2: 5	6	X	X	X	X	X	X	X
	7	X	X	X	X	X	X	X
	8	X	X	X	X	X	X	X
	9	X	X	X	X	X	X	X
	10	X	X	X	X	X	X	X
G3: 10	11	X	X	X	X	X	X	X

	12	X	X	X	X	X	X	X
	13	X	X	X	X	X	X	X
	14	X	X	X	X	X	X	X
	15	X	X	X	X	X	X	X
	16	X	X	X	X	X	X	X
	17	X	X	X	X	X	X	X
G4: 20	18	X	X	X	X	X	X	X
	19	X	X	X	X	X	X	X
	20	X	X	X	X	X	X	X

X- no mortality or morbidity observed

Table 4: Individual animal gross pathology

GROUP No: (mg/kg; b.wt)	**ANIMAL No.**	**TISSUES/ORGANS**	**OBSERVATION (INTERNAL & EXTERNAL)**
G1: 2.5	1	External orifices, body cavities- cranial, abdominal, and thoracic, lymph nodes, trachea, thyroid, thymus, lungs, heart, kidneys, adrenals, urinary bladder, testes, epididymis, liver, small and large intestines, spleen and eyes.	NAD
	2		NAD
	3		NAD
	4		NAD
	5		NAD
G2 ; 5	6		NAD
	7		NAD
	8		NAD
	9		NAD
	10		NAD
G3; 10	11		NAD
	12		NAD
	13		NAD

	14		NAD
	15		NAD
	16		NAD
	17		NAD
G4; 20	18		NAD
	19		NAD
	20		NAD

XENOGRAFT :

Tumour response to treatment:

Balb C nude mice were inducted and randomized into the study after the development of a tumour volume of 100mm^3. In short, at the end of the treatment period the overall tumour reduction was seen in the combination group. Images of animals bearing tumour (Fig.5A) along with the excised tumor (Fig. 5B) are shown for reference. Fig. 6 showcases the average of tumour changes during the treatment period. No animal in the control group survived for the full period of treatment. The carrier control group (ENG) showed survival but no reduction in tumour volume. The EZA group showed a transient reduction in tumour volume but at the end of 28 days, treatment effect was not profound. In contrast, the DEC group maintained a plateau, where the tumour had an initial growth phase but remained cut off from further development for the duration of the study. COMBO showed an interesting steady decrease in tumour volume at the end of the treatment period. The description pertains to the averages of the groups and variations within the group. Some animals were not inducted into the study due to no/insufficient development of tumour volume. A Kaplan Meier survival analysis (Fig. 7) has also been shown to have significance in treatment groups with the DEC and COMBO groups having higher survival rates. A detailed individual animal tumour volume tracking for the treatment period is provided in table 5.



Figure 7:Photographs of subcutaneous tumour induced in nude mice (A). B shows excised tumour at the end of treatment period.

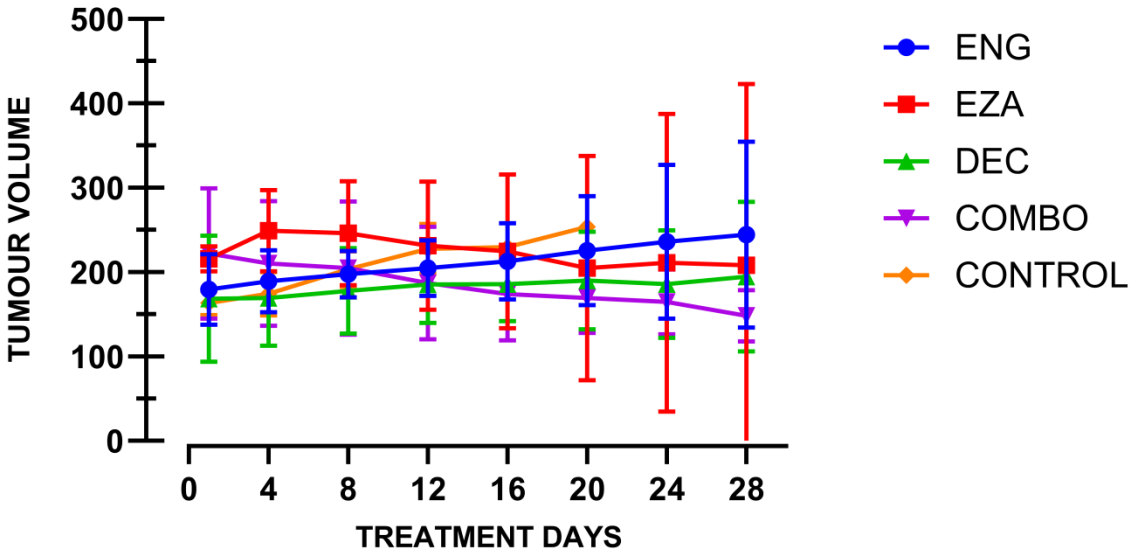


Figure 9:Two-way ANOVA analysis graph on tumour size in response to treatment observed against control for the treatment period

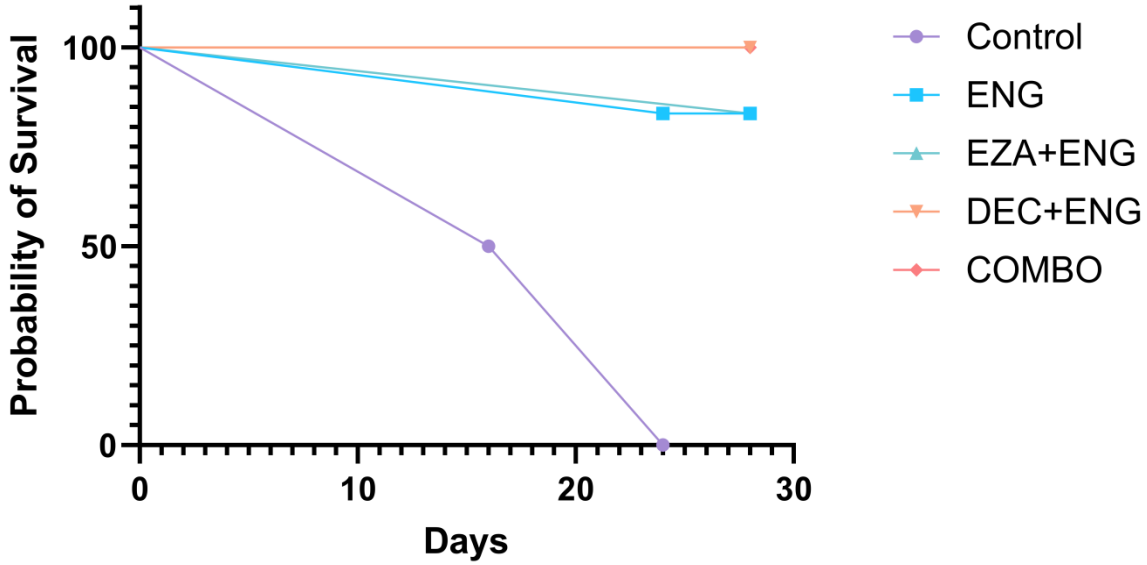


Figure 8:Kaplan- Meier survival analysis for nude mice during the treatment period of 28 days.

Table 5: Measurement of individual tumour volume in over the treatment period of 28 days

Group	A.No	Tumor confirmation Day 0	Treatment						
			Day 4	Day8	Day12	Day 16	Day20	Day24	Terminal day (day 28)
G1 Control	1	FD							
	3	151.47	156.21	203.3	230.54	D	D	D	D
	12	162.49	164.75	189.26	204.24	233.65	256.36	D	D
	14	184.16	212.68	233.72	268.42	D	D	D	D
	22	156.26	164.83	187.84	206.95	225.83	250.91	D	D
	Mean	163.595	174.6175	203.53	227.5375	229.74	253.64	NA	NA
	SD	14.43	25.70	21.30	29.70	5.53	3.85	NA	NA
G2 (Elastin Nanogel)	2	225.71	217.08	209.91	203.88	203.88	193.84	181.81	174.16
	5	167.59	197.65	220.91	243.42	269.65	303.95	347.60	372.21
	8	173.09	195.28	209.67	229.91	246.77	278.08	304.11	331.48
	16	137.55	151.96	166.71	184.46	197.28	245.62	D	D
	9	211.46	210.00	196.27	183.08	159.58	144.80	120.98	103.46
	6	118.95	125.60	150.99	163.29	184.46	207.91	225.04	240.71
	Mean	**172.39**	**182.93**	**192.41**	**201.34**	**209.23**	**229.03**	**235.91**	**244.40**
	SD	**41.14**	**36.10**	**27.59**	**30.53**	**41.03**	**58.44**	**91.35**	**110.37**
G3 (Nanogel+ Enzalutamide)	17	175.46	191.01	203.41	235.89	252.53	257.94	303.42	370.70
	11	236.11	230.39	202.77	181.48	166.64	149.67	127.77	102.83
	21	200.11	296.45	289.74	237.94	215.44	131.96	116.30	85.22
	15	214.38	279.89	307.96	336.44	357.06	404.22	475.90	529.84
	24	241.60	237.77	224.55	197.92	186.71	159.22	130.88	D
	13	212.76	190.22	183.73	169.94	160.32	133.97	124.15	114.80
	Mean	**213.40**	**237.62**	**235.36**	**226.60**	**223.12**	**206.16**	**213.07**	**240.68**
	SD	**24.20**	**44.09**	**51.17**	**60.58**	**73.92**	**107.72**	**147.34**	**199.71**
G4 (Nanogel + Decursin)	20	116.54	121.96	129.64	134.81	134.84	137.47	141.44	145.70
	27	160.29	163.82	174.34	187.90	195.65	196.02	201.18	214.89
	26	296.84	267.26	262.74	250.60	234.44	218.94	186.07	175.88
	7	114.62	149.65	168.78	203.84	218.70	268.69	282.95	334.64
	29	154.59	144.21	153.85	150.91	145.62	129.71	117.52	102.12
	18	FD							
	Mean	**168.58**	**169.38**	**177.87**	**185.61**	**185.85**	**190.17**	**185.83**	**194.64**
	SD	**74.72**	**56.75**	**50.50**	**45.68**	**44.04**	**58.01**	**63.84**	**88.48**
G5 (Nanogel + Combo)	19	142.94	145.75	137.77	140.58	148.70	161.44	167.34	170.49
	4	295.11	276.95	297.46	275.61	254.11	227.30	213.24	177.94
	23	169.59	147.40	141.08	131.01	130.86	128.37	119.90	118.14
	10	280.91	271.63	242.97	200.63	162.61	160.56	158.75	126.50
	25	FD							
	28	FD							
	Mean	**222.14**	**210.43**	**204.82**	**187.03**	**174.07**	**169.42**	**164.81**	**148.27**
	SD	**77.05**	**73.77**	**78.73**	**66.67**	**54.92**	**41.54**	**38.32**	**30.31**

Histopathology analysis:

Organs of interest were harvested for histopathological analysis to assess systemic toxicology and possible metastasis. Haematoxylin and eosin-stained sections of the tumour, prostate, liver, kidneys and pancreas were examined (Fig.9). Specifically the tumour response to treatment was analysed by mapping area of necrosis. No significant toxicity in the organ level was observed however; necrosis was seen in the tumour with the enzalutamide group showing highest degree.

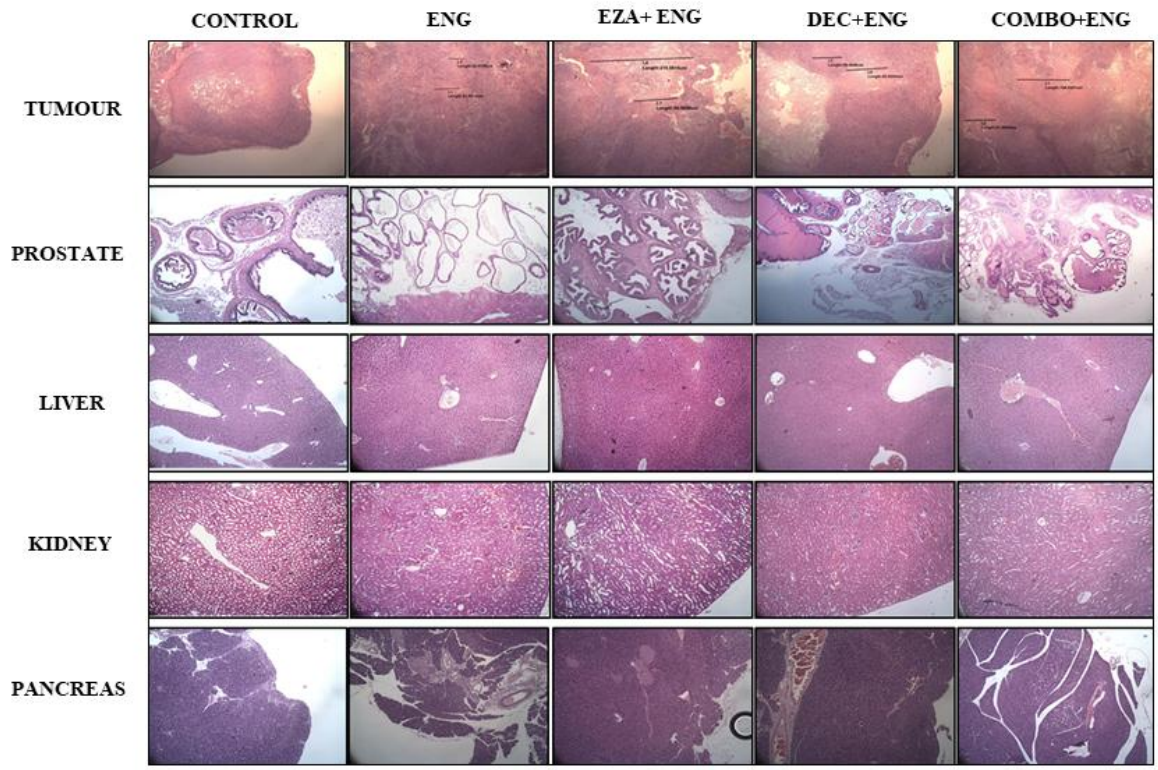


Figure 9: Routine H&E - stained sections of tumor along with organs of interest after treatment period.

Blood and Serum Biochemistry:

Signs of systemic damage and markers of organ failures and the blood count of animals in all groups were analysed. All studied parameters did not vary largely from the control, indicating safeness of treatment and insignificant drug or carrier induced damage. A full report of the parameters observed is presented in Tables 6 & 7.

Table 6: Hematology of xenograft mice treatment groups with reference range

GROUP	WBC	NEU	LYM	MON	EOS	BAS
Control	2.78 ± 0.34	1.86 ± 0.28	0.68 ± 0.21	0.12 ± 0.09	0.07 ± 0.00	0.02 ± 0.01

ENG	4.98 ± 1.70	2.05 ± 0.88	2.16 ±1.19	0.34 ±0.12	0.38 ± 0.28	0.02 ± 0.02
EZA+ENG	4.15 ± 1.80	1.56 ± 0.86	1.82 ± 1.36	0.38 ± 0.47	0.32 ± 0.39	0.08 ± 0.15
DEC+ENG	3.60 ± 1.87	1.23 ± 0.58	1.62 ± 1.20	0.23 ± 0.12	0.21 ± 0.17	0.01 ± 0.01
COMBO+ENG	3.37 ± 1.70	1.07 ± 0.30	1.86 ± 1.29	0.24 ± 0.09	0.19 ± 0.07	0.01 ± 0.01
Reference range	3.48 - 14.03	0.58 – 3.83	2.22 – 9.83	0.21 – 1.25	0.01 – 0.49	0.00 – 0.18

Table 7: Group averages of animal serum biochemical values

GROUP	UREA MG/DL	CREATININE MG/DL	ALT U/L	AST U/L
Control	10.43 ± 4.59	3.65 ± 0.78	79.58 ± 2.92	89.67 ± 12.01
ENG	11.74 ± 0.53	3.50 ± 1.93	78.70 ± 4.60	67.80 ± 16.84
EZA+ENG	17.10 ± 11.38	2.32 ± 1.47	85.81± 19.15	80.83± 38.24
DEC+ENG	44.66 ± 30.37	3.79 ± 1.97	83.55 ± 8.63	98.20 ± 27.91
COMBO+ENG	12.98 ± 1.75	1.35 ± 0.92	88.00 ± 17.11	45.75 ± 9.03
Reference range	15 – 55.6	0.2 – 0.4	41 - 131	55 - 352

DISCUSSION:

The present study demonstrates the potential of an elastin nanogel-based co-delivery system for enzalutamide and decursin in combating metastatic castration-resistant prostate cancer (mCRPC) using a DU145 xenograft model in BALB/c nude mice. Our findings reveal that the combination therapy, when encapsulated in the elastin nanogel (COMBO+ENG), elicits a more pronounced antitumor effect compared to monotherapy or vehicle controls, as evidenced by a steady reduction in tumor volume over the 28-day treatment period (Fig. 8 and Table 4). This aligns with the hypothesis that synergistic drug delivery can overcome enzalutamide resistance mechanisms, such as AR splice variants and alternative signaling pathways like NF-κB and STAT3, which decursin is known to modulate[13,18]. The observed plateau in tumor growth with decursin monotherapy (DEC+ENG) and transient reduction with enzalutamide monotherapy (EZA+ENG) underscore the complementary actions of these agents, where decursin's anti-proliferative, anti-angiogenic, and pro-apoptotic properties enhance enzalutamide's AR inhibition, potentially delaying resistance onset[11,19].

Decursin's multifaceted anti-cancer activity further bolsters the rationale for this combination. It downregulates androgen receptor expression and interferes with its transcriptional activity, diminishing survival signals critical for CRPC progression. Additionally, decursin induces G1-phase cell cycle arrest by downregulating cyclin D1 and upregulating p27/Kip1, preventing damaged cells from progressing through the cell cycle. Apoptosis is promoted via activation of caspase family members, leading to increased levels of cleaved PARP as a downstream marker of the intrinsic apoptotic cascade[18]. This broad-spectrum modulation of AR signaling,

cell cycle regulation, and apoptosis likely contributes to the superior tumor suppression observed in the COMBO+ENG group, including enhanced necrosis in treated tumors and improved survival (Fig. 8). In contrast to approved clinical PARP inhibitors (e.g., olaparib, rucaparib), which directly inhibit PARP enzymatic activity and exploit synthetic lethality in HRR-deficient tumors[29], decursin's effects on PARP are indirect—manifesting as cleavage during caspase-driven apoptosis rather than catalytic inhibition.

Rationale for EZA and DEC combination comes from the clinical and preclinical evidences available for both drugs individually. Upon investigating the association of EZA with DEC using STITCH analysis (Fig.3), it is well noted that these two drugs could be compatible in combination therapy. EZA's core function being AR blockade effectively does not prevent the progression to castration resistance. AR does not act in isolation, rather regulates genes involved in differentiation and proliferation. It functionally interacts with pathways that control plasticity and invasion. So, inhibiting just AR would not suffice and explains how adaptive rewiring of cellular processes takes place. β-catenin (CTNNB1) is a coactivator of AR which enables activation even at castrate levels of androgens. Unlike EZA, DEC seems to act in a way that disrupts the network that promotes plasticity, angiogenesis, epithelial- mesenchymal transition (EMT). AR in PCa being the hub of all other activity, makes What EZA does in PCa is tackle a vertical inhibition while DEC works on attenuating the horizontal pathways which rescue the cell from AR resistance. Characterization data further support the nanogel's suitability as a carrier. FTIR spectra confirmed successful drug loading without altering the elastin backbone, while DLS measurements indicated a consistent hydrodynamic diameter of approximately 160 nm across formulations, ideal for enhanced permeability and retention (EPR) in tumor tissues (Fig.1 and 2). The highly negative zeta potential (-55 mV)[30] suggests excellent colloidal stability, reducing aggregation and improving circulation time, which likely contributed to the targeted accumulation observed in vivo[31]. These physicochemical properties address common challenges in nanomedicine, such as poor solubility of enzalutamide. Safety assessments across models provide reassuring evidence of the formulation's tolerability. In zebrafish embryos, no significant impacts on mortality, hatching rates, or developmental morphology were noted up to the tested concentrations, consistent with the model's utility for rapid toxicity screening in nanomedicines[17]. Similarly, acute toxicity studies in Wistar rats revealed no mortality, clinical signs, or gross pathological abnormalities at doses up to 20 mg/kg, indicating a favorable safety margin for intraperitoneal administration. In the xenograft model, hematological and serum biochemical parameters remained largely within normal ranges across groups, with no overt organ toxicity in histopathology. The pronounced necrosis in enzalutamide-treated tumors suggests a potent cytotoxic response, though this was moderated in the combination group, possibly reflecting decursin's balanced apoptotic induction[32]. While these results are promising, certain aspects warrant critical consideration. The DU145 model, though androgen-independent and representative of CRPC, may not fully capture the heterogeneity of clinical mCRPC, including AR-dependent variants or bone metastases, which are prevalent in patients[15,33]. The use of BALB/c nude mice, while appropriate for xenograft engraftment, lacks a fully intact immune system, potentially underestimating immunogenic responses to the nanogel in immunocompetent hosts. Additionally, the biweekly intravenous dosing regimen achieved efficacy but could be

optimized for frequency or route to further minimize variability in tumor responses, as seen in individual animal data. The absence of pharmacokinetic profiling in this study limits insights into drug release kinetics in vivo, though the sustained antitumor effects imply effective controlled release, akin to graphene oxide-based systems for enzalutamide. These limitations notwithstanding, the elastin nanogel's biocompatibility and biodegradability position it as a versatile platform for multi-drug delivery, potentially extending to other phytocompounds or targeted therapies. Future investigations could incorporate patient-derived xenografts or orthotopic models to better mimic clinical scenarios, alongside biodistribution studies to quantify tumor-specific accumulation. Moreover, exploring molecular endpoints, such as AR-V7 expression or sphingolipid profiles, would elucidate the precise mechanisms of synergy and resistance circumvention.

CONCLUSION

In summary, this work advances nanogel-based combinatorial strategies for mCRPC by demonstrating enhanced efficacy and safety of enzalutamide-decursin co-delivery. By addressing resistance through multi-targeted modulation—including AR downregulation, cell cycle arrest, and caspase-mediated apoptosis—and targeted delivery, this approach holds translational promise, paving the way for refined therapies in advanced prostate cancer.

ACKNOWLEDGEMENTS

We thank Sri Ramachandra Institute of Higher Education and Research (SRIHER) for providing excellent infra structure at the Central Research Facility (CRF). We also thank the Central instrumentation facility at the University of Madras, for providing DLS and Zeta access. Ramachandra Innovation Centre BIRAC Bio-NEST Bioincubator, for access to the Leica Dmi8 Thunder imager.

AUTHOR CONTRIBUTIONS

Conceptualization, V.K.L.; methodology, J.Y.D, G.A.R, V.K.L.; software, J.Y.D.; validation, J.Y.D, V.K.L, .; formal analysis, J.Y.D, G.A.R.; investigation, J.Y.D, V.K.L.; resources, V.K.L,.; data curation, V.K.L, K.S.S, K.N, S.R ; writing original draft preparation, J.Y.D, V.K.L; writing –review and editing, J.Y.D, V.K.L, R.J; visualization, V.K.L; supervision, V.K.L,.; project administration ,V.K.L ; All authors have read and agreed to the published version of the manuscript.

ANIMAL ETHICS APPROVAL

The studies on animals were approved by the institutional ethics committee.
Zebrafish embryonic toxicity assessment: IAEC/67/SRIHER/785/2022
Acute toxicity of rats: IAEC/71/SRIHER/854/2023

Xenograft in athymic mice: IAEC/67/SRIHER/786/2022

FUNDING STATEMENT

This study is financially supported by the Department of Science and Technology (DST), SERB (Research Grant CRG/2021/001369) to V-KL and by Sri Ramchandra Institute of higher Education and Research through the Founder Udayar Chancellor fellowship to JYD

CONFLICT OF INTERESTS

The authors declare no conflict of interests.

REFERENCES

1. Chakrabarti, D. *et al.* The contemporary management of prostate cancer. *CA. Cancer J. Clin.* **75**, 552–586 (2025).
2. Lowrance, W. T. *et al.* Advanced Prostate Cancer: AUA/ASTRO/SUO Guideline PART I. *J. Urol.* **205**, 14–21 (2021).
3. Shore, N. D. *et al.* Improved Survival with Enzalutamide in Biochemically Recurrent Prostate Cancer. *N. Engl. J. Med.* **394**, 563–575 (2026).
4. Abdulsamad, S. A. Experimental treatment efficacy of dmrFABP5 on prostate cancer singly or in combination with drugs in use. *Am. J. Cancer Res.* **14**, 300–323 (2024).
5. Panja, S. *et al.* Mechanism-centric regulatory network identifies NME2 and MYC programs as markers of Enzalutamide resistance in CRPC. *Nat. Commun.* **15**, 352 (2024).
6. Blatt, E. B. & Raj, G. V. Molecular mechanisms of enzalutamide resistance in prostate cancer. *Cancer Drug Resist.* https://doi.org/10.20517/cdr.2019.25 (2019) doi:10.20517/cdr.2019.25.
7. Wang, Y. *et al.* Mechanisms of enzalutamide resistance in castration-resistant prostate cancer and therapeutic strategies to overcome it. *Br. J. Pharmacol.* **178**, 239–261 (2021).

8. Chandrasekaran, G. *et al.* Computational Modeling of complete HOXB13 protein for predicting the functional effect of SNPs and the associated role in hereditary prostate cancer. *Sci. Rep.* **7**, 43830 (2017).
9. Chandrasekaran, G. *et al.* In silico analysis of the deleterious nsSNPs (missense) in the homeobox domain of human *HOXB13* gene responsible for hereditary prostate cancer. *Chem. Biol. Drug Des.* **90**, 188–199 (2017).
10. Jiang, W. *et al.* Intravenous delivery of enzalutamide based on high drug loading multifunctional graphene oxide nanoparticles for castration-resistant prostate cancer therapy. *J. Nanobiotechnology* **18**, 50 (2020).
11. Wu, W. *et al.* Prostate Cancer Xenograft Inhibitory Activity and Pharmacokinetics of Decursinol, a Metabolite of *Angelica gigas* Pyranocoumarins, in Mouse Models. *Am. J. Chin. Med.* **45**, 1773–1792 (2017).
12. Singh, D., Sharma, Y., Dheer, D. & Shankar, R. Stimuli responsiveness of recent biomacromolecular systems (concept to market): A review. *Int. J. Biol. Macromol.* **261**, 129901 (2024).
13. Xiang, S. *et al.* Crosstalk of NF-κB/P65 and LncRNA HOTAIR-Mediated Repression of MUC1 Expression Contribute to Synergistic Inhibition of Castration-Resistant Prostate Cancer by Polyphyllin 1–Enzalutamide Combination Treatment. *Cell. Physiol. Biochem.* **47**, 759–773 (2018).
14. Mathur, A. *et al.* Subverting ER-Stress towards Apoptosis by Nelfinavir and Curcumin Coexposure Augments Docetaxel Efficacy in Castration Resistant Prostate Cancer Cells. *PLoS ONE* **9**, e103109 (2014).
15. Kostlan, R. J. *et al.* Clinically Relevant Humanized Mouse Models of Metastatic Prostate Cancer Facilitate Therapeutic Evaluation. *Mol. Cancer Res.* **22**, 826–839 (2024).

16. Wang, J. *et al.* Reciprocal regulation between RACGAP1 and AR contributes to endocrine therapy resistance in prostate cancer. *Cell Commun. Signal.* **22**, 339 (2024).
17. Letrado, P., De Miguel, I., Lamberto, I., Díez-Martínez, R. & Oyarzabal, J. Zebrafish: Speeding Up the Cancer Drug Discovery Process. *Cancer Res.* **78**, 6048–6058 (2018).
18. Chu, Y. *et al.* A comprehensive review of the anticancer effects of decursin. *Front. Pharmacol.* **15**, 1303412 (2024).
19. Singla, R. K. *et al.* Natural Products for the Management of Castration-Resistant Prostate Cancer: Special Focus on Nanoparticles Based Studies. *Front. Cell Dev. Biol.* **9**, 745177 (2021).
20. Karanika, S., Karantanos, T., Yin, J., Li, L. & Thompson, T. C. Novel anti-androgen receptor signaling agents: Understanding the mechanisms of resistance. *Asian J. Urol.* **1**, 30–39 (2014).
21. Pinto, F., Dibitetto, F., Ragonese, M. & Bassi, P. Mechanisms of Resistance to Second-Generation Antiandrogen Therapy for Prostate Cancer: Actual Knowledge and Perspectives. *Med. Sci.* **10**, 25 (2022).
22. Mout, L. *et al.* Continued androgen signalling inhibition improves cabazitaxel efficacy in prostate cancer. *EBioMedicine* **73**, 103681 (2021).
23. Rather, G. A. *et al.* Facile synthesis of elastin nanogels encapsulated decursin for castrated resistance prostate cancer therapy. *Sci. Rep.* **14**, 15095 (2024).
24. Sailer, V. *et al.* Experimental in vitro, ex vivo and in vivo models in prostate cancer research. *Nat. Rev. Urol.* **20**, 158–178 (2023).
25. Thangavel, C. *et al.* Improvement in Therapeutic Efficacy and Reduction in Cellular Toxicity: Introduction of a Novel Anti-PSMA-Conjugated Hybrid Antiandrogen Nanoparticle. *Mol. Pharm.* **15**, 1778–1790 (2018).

26. Bakhshan, M. A., Sheikhzadeh, S., Ramezanimoladehi, M., Pourkamalzadeh, M. & Sheikhzadeh, S. Nano-phytochemical-based formulations as promising opportunities for prostate cancer therapy and management: a comprehensive narrative review. *Med. Oncol.* **42**, 510 (2025).
27. Soni, S. *et al.* Herbal nanogels: Revolutionizing skin cancer therapy through nanotechnology and natural remedies. *Eur. J. Med. Chem. Rep.* **10**, 100126 (2024).
28. Akar, R. O., Ekremoğlu, M., Altinkaynak, C., Kutluay, B. P. & Ulukaya, E. Enhancing Anti-Angiogenic Therapy with Bevacizumab-Loaded Nanoflowers Through The Chorioallantoic Membrane Assay. Preprint at https://doi.org/10.21203/rs.3.rs-5430745/v1 (2024).
29. Zhang, M. *et al.* Androgen Receptor and Poly(ADP-ribose) Glycohydrolase Inhibition Increases Efficiency of Androgen Ablation in Prostate Cancer Cells. *Sci. Rep.* **10**, 3836 (2020).
30. Daniel, J. Y. *et al.* Biocompatibility and Toxicity Evaluation of an Elastin-Based Nanogel Carrier for Enzalutamide: Comprehensive Characterization, Controlled Release and Assessment in Zebrafish Embryos. *J. Appl. Toxicol.* jat.70082 (2026) doi:10.1002/jat.70082.
31. Soni, S. *et al.* Herbal nanogels: Revolutionizing skin cancer therapy through nanotechnology and natural remedies. *Eur. J. Med. Chem. Rep.* **10**, 100126 (2024).
32. Karanika, S., Karantanos, T., Yin, J., Li, L. & Thompson, T. C. Novel anti-androgen receptor signaling agents: Understanding the mechanisms of resistance. *Asian J. Urol.* **1**, 30–39 (2014).
33. Wang, Y. *et al.* MiR26a reverses enzalutamide resistance in a bone-tumor targeted system with an enhanced effect on bone metastatic CRPC. *J. Nanobiotechnology* **22**, 145 (2024).